Robotica (2010) volume 28, pp. 1057–1064. © Cambridge University Press 2010
doi:10.1017/S0263574709990919

Sound source tracking considering obstacle avoidance for a mobile robot

Naoki Uchiyama*, Shigenori Sano and Akihiro Yamamoto

Department of Mechanical Engineering, Toyohashi University of Technology, 1-1 Hibarigaoka, Tempaku, Toyohashi, Aichi 441-8580, Japan.

(Received in Final Form: December 14, 2009. First published online: January 18, 2010)

SUMMARY

Sound source tracking is an important function for autonomous robots, because sound is omni-directional and can be recognized in dark environment. This paper presents a new approach to sound source tracking for mobile robots using auditory sensors. We consider a general type of two-wheeled mobile robot that has wide industrial applications. Because obstacle avoidance is also an indispensable function for autonomous mobile robots, the robot is equipped with distance sensors to detect obstacles in real time. To deal with the robot's nonholonomic constraint and combine information from the auditory and distance sensors, we propose a model reference control approach in which the robot follows a desired trajectory generated by a reference model. The effectiveness of the proposed method is confirmed by experiments in which the robot is expected to approach a sound source while avoiding obstacles.

KEYWORDS: Sound source tracking; Obstacle avoidance; Mobile robot; Model reference control.

1. Introduction

Sensor fusion is one of the key technologies for realizing autonomous robotic systems. Because sound is omni-directional and can be recognized in dark environments, combining the auditory sensor with others, such as visual sensors, will provide effective recognition of the robot's working environment. Many studies have examined sound source localization and tracking. Webb built an auditory sensor system based on the cricket ear and neural control, and examined the effectiveness for robot phonotaxis.[1] Faller and Merimaa presented a sound source localization method based on interaural coherence for complex listening situations where reflections and superposition effect of concurrently arriving sound are considered.[2] Murray *et al.* proposed a hybrid system incorporating cross-correlation and recurrent neural network for robot sound source tracking.[3] Woo-han *et al.* presented a method for impulse (footstep) sound source tracking using Kalman filter.[4] Because different sensor fusion may provide effective recognition of environment, combinatorial use of auditory and visual sensors for sound localization is also studied.[5–7] Detection of a three-dimensional position of sound source by two microphones like the human's ear is also a topic in this area.[8,9] Sound source localization and tracking have wide industrial and in-house applications, because they enable robots to approach objects difficult to recognize from a distant position. Approaching the object using auditory sensors enables the use of visual sensors for detail recognition.

This paper presents an approach to sound source tracking for a general type of two-wheeled mobile robot. Although obstacle avoidance is an indispensable function for mobile robots, it is not considered in the above studies. Because obstacles disturb not only the robot's motion but also the passage of sound, these two functions should be considered simultaneously in the robot controller. The two-wheeled mobile robot considered in this study is equipped with two microphones for sound source localization and several inexpensive infrared distance sensors to detect obstacles in unknown environments. The nonholonomic constraint needs to be considered, because it does not allow the two-wheeled mobile robot to move in an arbitrary direction.

Much research has been conducted on obstacle avoidance in mobile robots.[10–14] The dynamic window approach is one of the most efficient approaches that can take into account the nonholonomic constraint and be applied to unknown environments.[15,16] In this approach, the destination of the mobile robot is given and the robot motion is generally determined to optimize a certain cost function, such as the distance to the destination. In the sound source tracking problem, the direction from which the sound comes changes frequently with respect to the obstacle conditions, and hence the obstacle avoidance controller should be designed to respond flexibly to the changes.

There are some studies on sound source tracking with an obstacle avoidance function for mobile robots. Huang *et al.* presented a real time sound localization system for a mobile robot equipped three microphones and sonar system for obstacle avoidance.[17] Bicho *et al.* proposed an attractor dynamics approach to phonotaxis of a robot with five microphones and seven infrared sensors.[18] Andersson *et al.* developed a phonotaxis system that relies on diffraction about a human's head model with only two microphones.[19] However, robot dynamics are not considered in these approaches. In addition, the validity of these approaches is not discussed from the viewpoint of stability and positional analyses.

In this study, to simultaneously realize sound source tracking and obstacle avoidance, we propose a model

* Corresponding author. E-mail: uchiyama@mech.tut.ac.jp

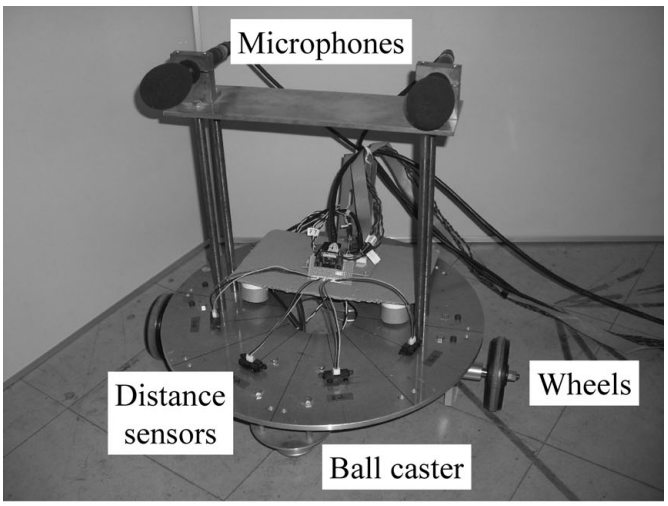

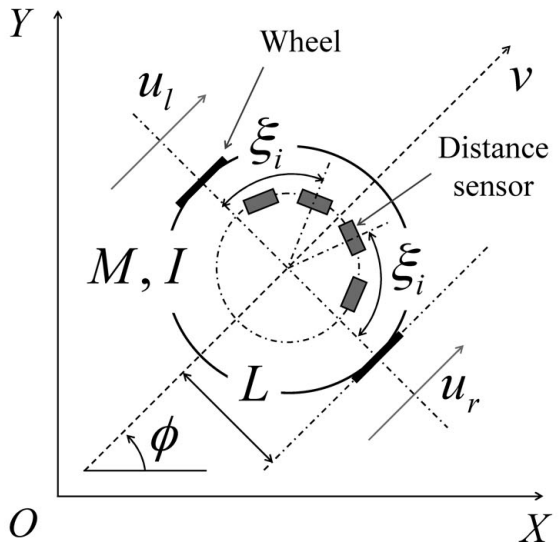

Fig. 1. Two-wheeled robot.

reference control approach, in which a dynamic model of the mobile robot with these two functions is employed. The reference model generates the desired wheel velocities that realize these two functions and satisfy the nonholonomic constraint. Stability and positional analyses are given to show the validity of the proposed approach. The effectiveness of the proposed approach is demonstrated by experimental results.

2. Mobile Robot with Sensors

In this study, we consider the control of a general type of two-wheeled mobile robot with two microphones and several distance sensors, as shown in Fig. 1. The dynamics of the robot is given as follows:

$$I\ddot{\phi} = (u_r - u_l)L, \tag{1}$$

$$M\dot{v} = u_l + u_r, \tag{2}$$

where I and M are the inertia and mass of the robot, respectively, u_l and u_r are the driving forces generated by the left and right wheels, respectively. L is the half-distance between the two wheels, and v and ϕ are the robot's translational speed and rotation angle, respectively.

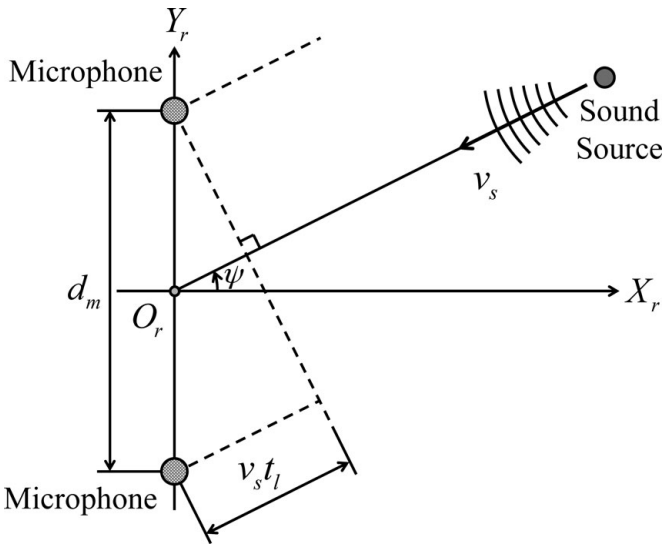

Fig. 2. Geometrical relationship between sound source and microphones.

Distance sensors for detection of obstacles are located symmetrically with respect to the centreline parallel to the translational direction of the robot, as shown in Fig. 1. Because the sensor has not only upper but also lower bounds of measurable distance, it is placed 7 cm inside the circumference of the robot body. The direction towards each sensor from a line that links the wheel centres is denoted by ξ_i.

The relationships between v, $\dot{\phi}$ and the wheel velocities are represented as

$$R_w\dot{\theta}_r = v + L\dot{\phi}, \tag{3}$$

$$R_w\dot{\theta}_l = v - L\dot{\phi}, \tag{4}$$

where R_w is the radius of each wheel, and θ_l and θ_r are the left and right wheel rotational angles, respectively.

3. Controller Design

3.1. Sound source localization

In this study, we employ the interaural time difference (ITD) and level difference (LD) to localize sound sources. Although the interaural level difference (ILD) is considered for sound localization in some studies (e.g., [2, 19]), we use the sound level difference between the desired and current positions, because the distance between the two microphones is too small to recognize the ILD in our small robot. Figure 2 shows the geometrical relationship between the microphones and the sound source. The origin of the coordinate system O_r is located between the two microphones on the robot, and ψ denotes the direction to the sound source from the origin. d_m is the distance between the two microphones, and v_s is the

https://doi.org/10.1017/S0263574709990919 Published online by Cambridge University Press

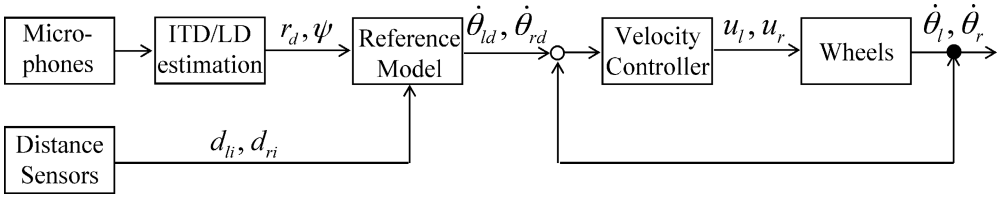

Fig. 3. Block diagram of model reference control system.

speed of sound. We have the following relation from Fig. 2,

$$\psi = \arcsin\left(\frac{v_s t_l}{d_m}\right), \tag{5}$$

where t_l is the difference in the sound wave arrival time between the two microphones. Hence, we can detect the direction of the sound source ψ by estimating the value of t_l. We employ the following cross-correlation function to estimate the value of t_l,

$$\begin{aligned} S(\tau) &= \frac{\langle L(t+\tau), R(t)\rangle}{\|L(t)\|\|R\|}, \\ \langle L(t+\tau), R(t)\rangle &= \lim_{T\to\infty}\frac{1}{T}\int_0^T L(t+\tau)R(t)\mathrm{d}t, \\ \|L(t)\| &= \sqrt{\lim_{T\to\infty}\frac{1}{T}\int_0^T L^2(t)\mathrm{d}t}, \\ \|R(t)\| &= \sqrt{\lim_{T\to\infty}\frac{1}{T}\int_0^T R^2(t)\mathrm{d}t}, \end{aligned} \tag{6}$$

where $L(t)$ and $R(t)$ denote time-series signals obtained from the left and right microphones, respectively. t is the time when the cross-correlation function is calculated, and τ is the shift from the time t. Calculating the value $S(\tau)$ by changing the value of τ for a certain range, we estimate the value of t_l as follows, because $S(\tau)$ provides the similarity of the two signals $L(t+\tau)$ and $R(t)$:

$$t_l = \arg\max_{\tau}\{S(\tau)\}. \tag{7}$$

The LD l_d relates to the distances between the sound source position and the current and desired robot positions as,

$$l_d = 20\log\frac{r_d}{r_s}, \tag{8}$$

where r_d denotes the distance between the sound source and the robot (the origin of the coordinate frame in Fig. 2), and r_s is the distance between the sound source and the desired robot position. Assigning the value of r_s, which designates the distance that should remain between the robot and the sound source, we can estimate the value of r_d from l_d. We employ the average of the sound levels of two microphones for the value of l_d.

3.2. Model reference control approach

Because the robot cannot move in arbitrary directions due to a nonholonomic constraint, we propose a control algorithm based on the model below. It has a dynamics similar to that of the mobile robot except for the obstacle avoidance and sound tracking functions,

$$I\ddot{\phi} + C_\phi\dot{\phi} = k_\phi\psi + \sum_{i=1}^{m}(\alpha_i \mathrm{e}^{-nd_{ri}}) - \sum_{i=1}^{m}(\alpha_i \mathrm{e}^{-nd_{li}}), \tag{9}$$

$$M\dot{v} + C_v v = k_v(r_d - r_s) - \sum_{i=1}^{m}(\beta_i \mathrm{e}^{-nd_{ri}}) - \sum_{i=1}^{m}(\beta_i \mathrm{e}^{-nd_{li}}), \tag{10}$$

where C_ϕ and C_v are the viscous friction coefficients for increasing the systems's stability, d_{li} or d_{ri} are the distances between the sensor at angle ξ_i, and the obstacle, where the subscripts l and r indicate the sensor located at the left and right wheel, respectively. m denotes half the number of sensors. The first term on the right-hand side of Eq. (9), where k_ϕ is a constant controller gain, gives the effect of making the robot turn to the sound source. The last two terms on the right-hand side of Eq. (9) give the effect of steering for avoiding the obstacle. The magnitude of steering depends on the distances to the obstacle d_{li} and d_{ri}. The first term on the right-hand side of Eq. (10), where k_v is a constant controller gain, makes the robot approach the sound source. The last two terms on the right-hand side of Eq. (10) act as a brake. The magnitude of the braking force also depends on the distances to the obstacle. Parameters α_i, β_i and n are constants for changing the effects of these steering and brake-like functions.

Nonholonomicity is considered in this design because the model in Eqs. (9) and (10) is based on the original robot dynamics. As the dynamics expression in Eqs. (1) and (2) and the actuator dynamics of the robot generally have modelling errors and are affected by disturbances, we propose a model reference control approach as shown in Fig. 3, where the desired wheel (motor) velocities $\dot{\theta}_{ld}$ and $\dot{\theta}_{rd}$ are generated using the sound source information r_d and ψ, the distance sensor information d_{li} and d_{ri}, and Eqs. (9) and (10). The velocity controller block in Fig. 3 enables the wheel angular velocities, $\dot{\theta}_l$ and $\dot{\theta}_r$, to track $\dot{\theta}_{ld}$ and $\dot{\theta}_{rd}$, respectively. The control system in Fig. 3 can be made robust to plant modelling errors and disturbances by designing robust wheel velocity controllers. Because many techniques exist for designing robust wheel (motor) controllers (e.g., [20]), we can apply any of them to the control system in Fig. 3.

https://doi.org/10.1017/S0263574709990919 Published online by Cambridge University Press

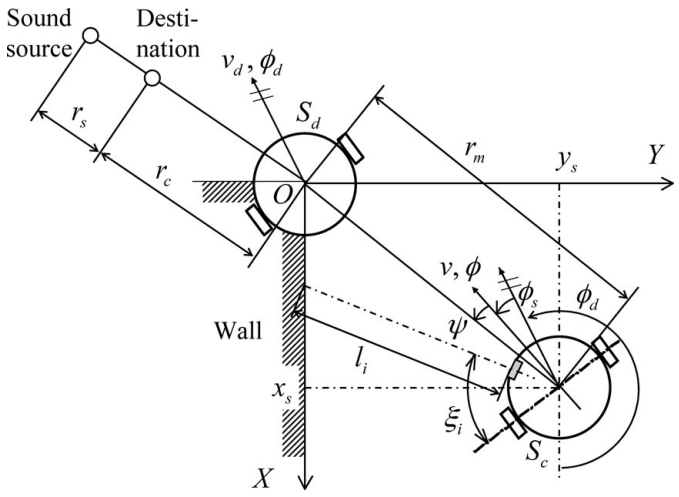

Fig. 4. Model for stability and positional analysis.

This model reference control approach may be applied to obstacle avoidance problem for other types of robotic systems such as four-wheeled mobile robots and robotic manipulators because the reference model inherits the property of original robot dynamics and provides appropriate motion for the robot.

3.3. Stability and positional analysis

To verify the effectiveness of the proposed controller design, for simplicity, we consider the case in Fig. 4, where the robot is expected to approach the sound source while avoiding collision with a wall. The state S_c denotes the current robot position. The sound from the source is diffracted by the wall, and hence the robot first approaches the state S_d. We assume that this is the intermediate desired state, and its velocity v_d and orientation ϕ_d are constants, i.e., $\dot{v}_d = 0$ and $\dot{\phi}_d = 0$. To employ a linear analysis for simplicity, we denote X, Y and ϕ directional deviations from the desired state to the current one by x_s, y_s and ϕ_s, respectively. In addition, only wall side sensors of the robot are considered in this analysis.

The distance from the wall to the ith sensor is given by

$$l_i = \frac{y_s}{\cos(\xi_i - \phi_d - \phi_s + \pi)} - L. \tag{11}$$

This equation is linearized as

$$l_i \simeq -\frac{y_s}{\cos(\xi_i - \phi_d)} - L. \tag{12}$$

Because only wall-side sensors are considered, Eqs. (9) and (10) are written as

$$I\ddot{\phi} + C_\phi\dot{\phi} = k_\phi\psi - \textstyle\sum_{i=1}^{m}(\alpha_i \mathrm{e}^{-nd_{ri}}), \tag{13}$$

$$M\dot{v} + C_v v = k_v(r_d - r_s) - \textstyle\sum_{i=1}^{m}(\beta_i \mathrm{e}^{-nd_{ri}}). \tag{14}$$

The term $\mathrm{e}^{-nd_{ri}}$ is linearized as

$$\mathrm{e}^{-nd_{ri}} \simeq -p_i l_i + q_i, \tag{15}$$

where p_i and q_i are positive constants. From Fig. 4,

$$\psi + \phi_s = C, \tag{16}$$

where C is a positive constant. We have the following relation with the velocity of the robot v.

$$\begin{aligned} v &= v_d + v_s \\ &= \dot{x}\cos(\phi_d + \psi_s) + \dot{y}\sin(\phi_d + \psi_s) \\ &\simeq \dot{x}_d\cos\phi_d + \dot{y}_d\sin\phi_d - (\dot{x}_d\sin\phi_d - \dot{y}_d\cos\phi_d)\phi_s \\ &\quad + \dot{x}_s\cos\phi_d + \dot{y}_s\sin\phi_d, \end{aligned} \tag{17}$$

where v_s is a deviation from the desired velocity. $(x_d,\ y_d)$ and $(x,\ y)$ are the desired and current robot positions, respectively. Applying the relation

$$v_d = \dot{x}_d\cos\phi_d + \dot{y}_d\sin\phi_d \tag{18}$$

and a nonholonomic constraint

$$\dot{x}_d\sin\phi_d - \dot{y}_d\cos\phi_d = 0 \tag{19}$$

to Eq. (17), we have

$$v = v_d + \dot{x}_s\cos\phi_d + \dot{y}_s\sin\phi_d. \tag{20}$$

Differentiating Eq. (20) with respect to time, we have

$$\dot{v} = \dot{v}_d + \ddot{x}_s\cos\phi_d + \ddot{y}_s\sin\phi_d. \tag{21}$$

Length r_m in Fig. 4 is represented as

$$r_m = -x_s\sin(\phi_d + \phi_s + \psi) - y_s\cos(\phi_d + \phi_s + \psi), \tag{22}$$

and linearized as follows:

$$r_m \simeq -(x_s\cos\phi_d + y_s\sin\phi_d). \tag{23}$$

Substituting Eqs. (12), (15), (16), (21) and (23) into Eqs. (13) and (14), we have

$$\begin{aligned} &I\ddot{\phi}_s + C_\phi\dot{\phi}_s = k_\phi(-\phi_s + C) \\ &\quad - \sum_{i=1}^{m}\alpha_i\left\{-p_i\left(-\frac{y_s}{\cos(\xi_i - \phi_d)} - L\right) + q_i\right\}, \end{aligned} \tag{24}$$

$$\begin{aligned} &M(\ddot{x}_s\cos\phi_d + \ddot{y}_s\sin\phi_d) + C_v(v_d + \dot{x}_s\cos\phi_d + \dot{y}_s\sin\phi_d) \\ &= k_v(-x_s\cos\phi_d - y_s\sin\phi_d) + k_v r_c \\ &\quad - \sum_{i=1}^{m}\beta_i\left\{-p_i\left(-\frac{y_s}{\cos(\xi_i - \phi_d)} - L\right) + q_i\right\}, \end{aligned} \tag{25}$$

Linearizing the nonholonomic constraint

$$(\dot{x}_d + \dot{x}_s)\sin(\phi_d + \phi_s) - (\dot{y}_d + \dot{y}_s)\cos(\phi_d + \phi_s) = 0 \tag{26}$$

and considering Eqs. (18) and (19), we get

$$\ddot{x}_s\sin\phi_d - \ddot{y}_s\cos\phi_d + v_d\dot{\phi}_s = 0. \tag{27}$$

https://doi.org/10.1017/S0263574709990919 Published online by Cambridge University Press

Equations (24), (25) and (27) can be represented in the following state space form:

$$\dot{z} = Az + h, \tag{28}$$
$$z = \left[z_1 \ \cdots \ z_6 \right]^T,$$

$$A = \begin{bmatrix} & O_{3\times3} & & & I_{3\times3} & \\ -\frac{k_p}{I} & 0 & -\frac{a}{I} & -\frac{C_\phi}{I} & 0 & 0 \\ 0 & \frac{c^2k_v}{M} & -\frac{csk_v+bc}{M} & -sv_d & -\frac{c^2C_v}{M} & -\frac{csC_v}{M} \\ 0 & \frac{-csk_v}{M} & -\frac{s^2k_v+bs}{M} & cv_d & -\frac{csC_v}{M} & -\frac{s^2C_v}{M} \end{bmatrix},$$

$$c = \cos\phi_d,\ s = \sin\phi_d,\ a = \sum_{i=1}^{m} \frac{\alpha_i p_i}{\cos(\xi_i - \phi_d)},$$

$$b = \sum_{i=1}^{m} \frac{\beta_i p_i}{\cos(\xi_i - \phi_d)}$$

$$h = \left[0 \quad 0 \quad 0 \quad k_\phi C - \sum_{i=1}^{m} \alpha_i (p_i L + q_i) \quad -C_v v_d + k_v r_c - \sum_{i=1}^{m} \beta_i (p_i L + q_i) \quad 0 \right]^T,$$

where $z_1 = \phi_s, z_2 = x_s,\ z_3 = y_s,\ z_4 = \dot{\phi}_s,\ z_5 = \dot{x}_s$ and $z_6 = \dot{y}_s$, and $O_{3\times3}$ and $I_{3\times3}$ are the 3×3 zero and identity matrices, respectively. We can check the stability of the linearized control system by calculating eigenvalues of A. Note that two uncontrollable modes remain even when the controller gains are appropriately adjusted in A. This is because only two values, ψ and r_d, are fed back, and the lateral direction of the robot cannot be controlled.

Assuming that all controllable modes in Eq. (28) are stabilized (i.e., $\ddot{\phi}_s = 0,\ \dot{\phi}_s = 0,\ \ddot{x}_s \cos\phi_d + \ddot{y}_s \sin\phi_d = 0$, and $\dot{x}_s \cos\phi_d + \dot{y}_s \sin\phi_d = 0$ are achieved), we find values of y_s and ϕ_s at $x_s = 0$ (i.e., robot position is on the Y-axis in Fig. 4). From Eq. (25), we have

$$C_v v_d + \sum_{i=1}^{m} \beta_i (p_i L + q_i) - k_v r_c = \left(-k_v \sin\phi_d - \sum_{i=1}^{m} \frac{\beta_i p_i}{\cos(\xi_i - \phi_d)} \right) y_s \tag{29}$$

If we assign large values to β_i, then the left-hand side of Eq. (29) has a positive value. Because the coefficient of y_s is positive on the right-hand side of Eq. (29), we conclude that y_s is positive at $x_s = 0$. To achieve the obstacle avoidance, the robot body size needs to be considered (i.e., $y_s > L$). Assuming that the same value is used for all β_i's (i.e., $\beta_i = \beta$), we have $\mathrm{d}y_s/\mathrm{d}\beta$ as follows:

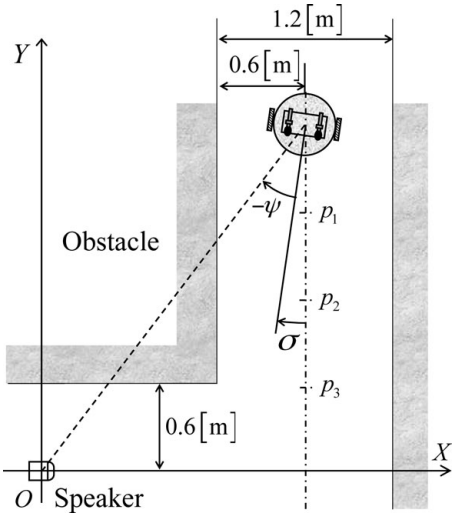

Fig. 5. Experimental environment.

$$\frac{\mathrm{d}y_s}{\mathrm{d}\beta} = \frac{-\sum_{i=1}^{m}(p_i L + q_i)k_v \sin\phi_d + \sum_{i=1}^{m} \frac{p_i}{\cos(\xi_i - \phi_d)}(C_v v_d - k_v r_c)}{\left(-k_v \sin\phi_d - \beta \sum_{i=1}^{m} \frac{p_i}{\cos(\xi_i - \phi_d)} \right)^2} \tag{30}$$

Since q_i has a large value generally, y_s is concluded to be monotonically increasing with respect to β. Hence, by increasing the value of β, we can achieve $y_s > L$.

From Eq. (24), we have

$$k_\phi \phi_s = k_\phi C - \sum_{i=1}^{m} \alpha_i \left\{ -p_i \left(-\frac{y_s}{\cos(\xi_i - \phi_0)} - L \right) + q_i \right\} \tag{31}$$

Hence $\phi_s < 0$ if large values are assigned to α_i.

From the above facts, it can be concluded that the robot avoids the wall and receives sound directly from the sound source at $x_s = 0$ (i.e., on the Y-axis). From this position, the robot can approach the sound source directly and hence control objective can be achieved.

4. Experiments

The proposed controller design is experimentally verified in the environment shown in Fig. 5, where the robot is

https://doi.org/10.1017/S0263574709990919 Published online by Cambridge University Press

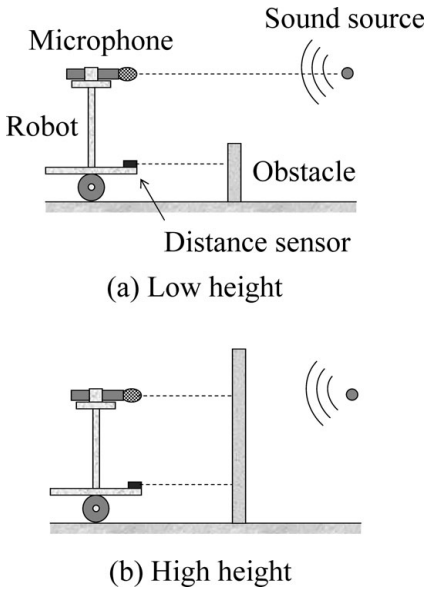

Fig. 6. Obstacle conditions.

expected to approach the speaker. The following three obstacle conditions are considered.

(a1) No obstacle
(a2) Obstacle that disturbs robotic motion.
(a3) Obstacle that disturbs robotic motion and sound passage.

Figure 6 shows the difference between (a2) and (a3), where the height of the obstacle is different in (a) and (b).

Random noise at a magnitude of 80 [dB] is employed for the sound source. The constant parameters used in this experiment are given in Table I. The parameter values for the obstacle avoidance are determined in a trial-and-error manner by simulation. DC servo motors (20 [W]) are employed for each wheel's motion. Rotary encoders (500 [PPR]) attached to the motors are used for measuring the robot's position and orientation. The measurable range of the distance sensor is 4–80 [cm].

Figure 7 shows a plot of eigenvalues of A in Eq. (28) with the parameters in Table I. In this plot, ϕ_d, v_d, p_i, k_v and k_ϕ are changed as $\phi_d = 195$–$255[^\circ]$ by 20°, $v_d = 0.05$–0.2[m/s] by 0.05[m/s], $p_i = 0.2$–1.4[N/m] by 0.4[N/m], $k_v = 1$–21[Nm] by 5[Nm] and $k_\phi = 1$–21[Nm/rad] by 5[Nm/rad], respectively. Because all eignevalues except the uncontrolled ones are always in the left half of the complex plane, the proposed controller provides a stable feedback system. (Uncontrolled eigenvalues are located on the imaginary axis.)

First, we have placed the robot at the configuration $p_1 = [1.8,\ 1.8]$ [m] and $\sigma = 0$ [deg], and conducted the

Table I. Parameter values of the experimental system.

M	9.6 [kg]	I	0.24 [kg m^2]
C_v	5.0 [Nm/s]	C_ϕ	1.25 [Nm/(rad/s)]
L	0.25 [m]	n	10
α_1	6.0	β_1	3.0
α_2	3.6	β_2	1.8
k_ϕ	3.0 [Nm/rad]	k_v	5.0 [N/m]
d_m	0.3 [m]	R_w	0.03 [m]

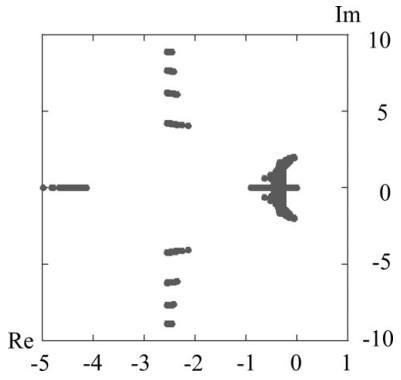

Fig. 7. Control system poles.

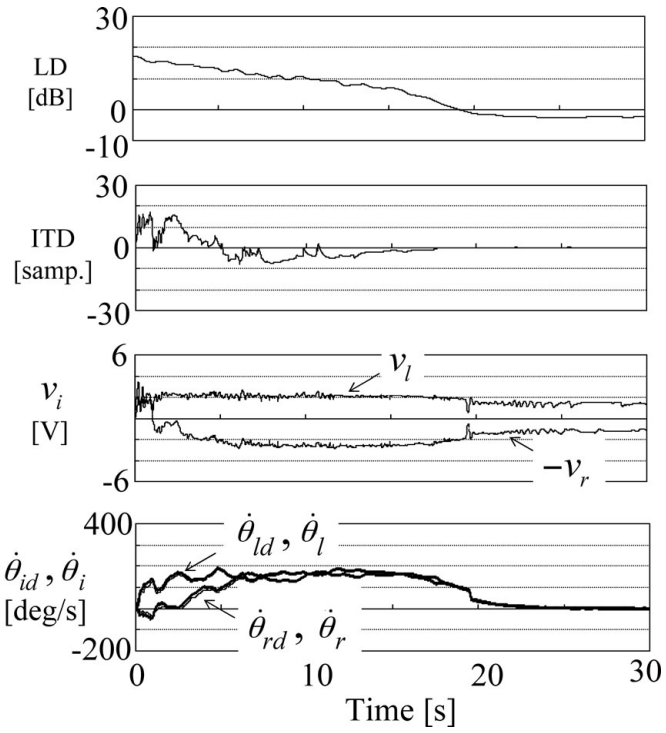

Fig. 8. Experimental results (no obstacle, initial configuration: $p_1 = [1.8,\ 1.8]$ [m], $\sigma = 0$ [deg]).

experiment. The experimental results for obstacle conditions (a1)–(a3) are given in Figs. 8–10, where v_l and v_r are control input voltages that are proportional to u_l and u_r, respectively. In all cases, the robot successfully approached the speaker, and both the LD and ITD converged to around zero. In Figs. 8 and 9, the ITD has a higher value around the starting point than in Fig. 10, because the sound passage in the first two cases is not disturbed, and hence the robot can recognize the direction to the sound source. On the other hand, in Figs. 9 and 10, the wheel angular velocities $\dot{\theta}_l$ and $\dot{\theta}_r$ show different profiles compared to those in Fig. 8 as it avoided the obstacle. In particular, the left wheel velocity $\dot{\theta}_l$ has a larger magnitude than the right one to make the right turn. In all cases, the wheel velocities well follow the desired ones generated by the reference model. These results confirms the effectiveness of the proposed model reference control approach.

Table II summarizes the experimental results in which the initial positions and orientations are changed from p_1 to p_3 and $\sigma = 0$ to 90 [deg] by 45 [deg], respectively. The robot fails to approach the speaker in some initial configurations.

https://doi.org/10.1017/S0263574709990919 Published online by Cambridge University Press

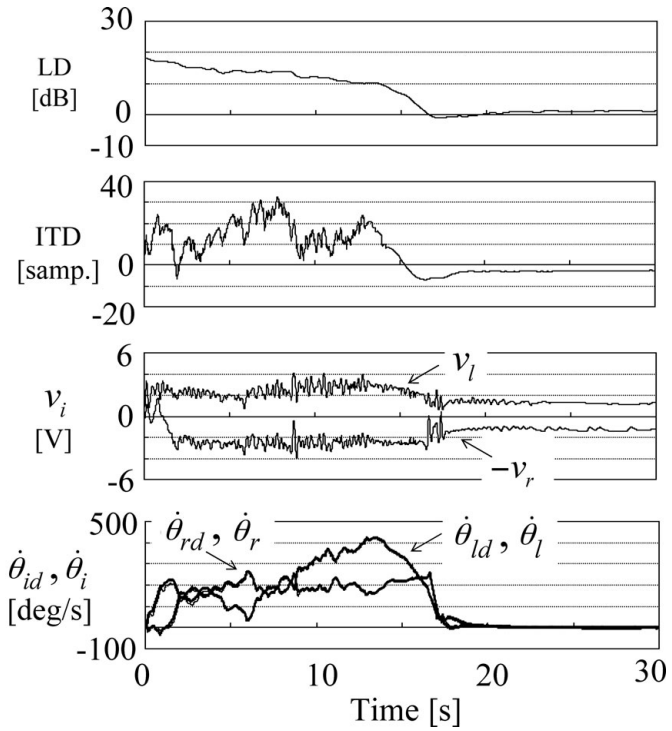

Fig. 9. Experimental results (low height obstacle, initial configuration: $p_1 = [1.8,\ 1.8]$ [m], $\sigma = 0$ [deg]).

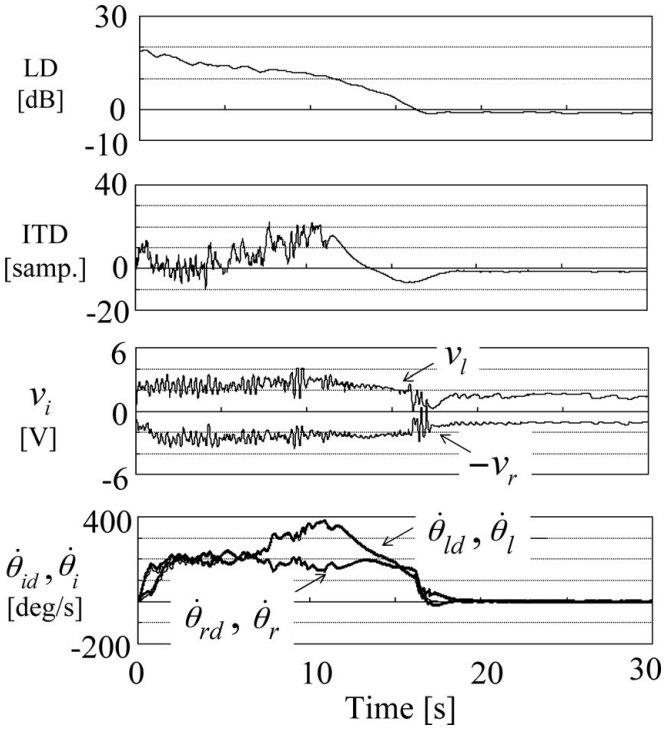

Fig. 10. Experimental results (high height obstacle, initial configuration: $p_1 = [1.8,\ 1.8]$ [m], $\sigma = 0$ [deg]).

When the initial position is at p_3, it is difficult to recognize the corner of the obstacle, because it is in the distance sensor's blind spot. In addition, when $\sigma = 90$ [deg], the robot may turn to the right, making the sound recognition impossible. These two causes of failure can be removed by increasing the number of sensors or using laser range sensors.

Table II. Summary of experimental results (◯: succeeded, ×: failed, initial positions [m]: $p_1 = [1.8,\ 1.8]$, $p_2 = [1.8,\ 1.2]$, $p_3 = [1.8,\ 0.6]$).

			σ [deg]		
No.	Obstacle	Init. pos.	0	45	90
1	None	p_1	◯	◯	◯
2		p_2	◯	◯	◯
3		p_3	◯	◯	◯
4	Low	p_1	◯	◯	◯
5		p_2	◯	◯	◯
6		p_3	×	×	×
7	High	p_1	◯	◯	×
8		p_2	◯	◯	×
9		p_3	◯	×	×

5. Conclusions

This paper presents a new approach to sound source tracking and obstacle avoidance for two-wheeled mobile robots using two microphones and inexpensive infrared distance sensors. Because the proposed method is based on a model reference control approach, it can consider the nonholonomic constraint of a mobile robot and be made robust to plant modelling errors and disturbances. The experimental results demonstrate the effectiveness of the proposed approach, where the robot is able to avoid the obstacle and approach the sound source except when they are in the sensor's blind spot. Future works include extension of the presented linear analysis to more general cases, applying the proposed robot system to more complicated environment after considering the problem of sensor blind spot and extending the proposed model reference control for other types of mobile robots and robotic manipulators.

References

1. B. Webb, "Robots, crickets and ants: Models of neural control of chemotaxis and phonotaxis," *Neural Netw.* **11**, 1479–1496 (1998).
2. C. Faller and J. Merimaa, "Sound localization in complex listening situations: Selection of binaural cues based on interaural coherence," *J. Acoust. Soc. Am.* **116**(5), 3075–3089 (2004).
3. J. Murray, S. Wermter and H. Erwin, "Auditory robotic tracking of sound sources using hybrid cross-correlation and recurrent networks," *Proc. 2005 IEEE/RSJ International Conference on Intelligent Robots and Systems*, (2005) pp. 3554–3559.
4. Y. Woo-han, O. Cheon-in, B. Kyu-Dae and J. Su-young, "The impulse sound source tracking using kalman filter and the cross-correlation," *Proc. International Joint Conference SICE-ICASE*, (2006) pp. 317–320.
5. K. Nakadai, K.Hidai, H. G. Okuno, H. Mizoguchi and H. Kitano, "Real-time auditory and visual multiple-speaker tracking for human-robot interaction," *IEEE J. Robot. Mechatronics*, 479–489, JSME (2002).
6. H. G. Oguno, K. Nakadai, T. Lourens and H. Kitano, "Sound and visual tracking for humanoid robot," *Appl. Intell.* **20**, 253–266 (2004).
7. X. Lv, M. Zhang and X. Liu, "A sound source tracking system based on robot hearing and vision," *Proc. 2008 International Conference on Computer Science and Software Engineering*, (2008) pp. 1119–1122.
8. J. Hörnstein, M. Lopes, J. Santos-Victor and F. Lacerda, "Sound localization for humanoid robots-building

https://doi.org/10.1017/S0263574709990919 Published online by Cambridge University Press

Audio-motor maps based on the HRTF," *IEEE/RSJ International Conference on Intelligent Robots and Systems*, (2006).
9. J. F. Ferreira, C. Pinho and J. Dias, "Implementation and calibration of a bayesian binaural system for 3D localisation," *2008 IEEE International Conference on Robotics and Biomimetics*, (2008).
10. O. Khatib, "Real-time obstacle avoidance for fast mobile robots," *Int. J. Robot. Res.* **5**(1), 90–98 (1986).
11. J. C. Latombe, *Robot Motion Planning* (Kluwer Academic Publishers, 1991).
12. A. Chakravarthy and D. Ghose, "Obstacle avoidance in a dynamic environment: A collision cone approach," *IEEE Trans. Syst. Man Cybern.* **28**(5), 562–574 (1998).
13. J. Borenstein and Y. Koren, "Real-time obstacle avoidance for fast mobile robots," *IEEE Trans. Syst. Man Cybern.* **19**(5), 1179–1187 (1989).
14. F. Lamiraux, D. Bonnafous and O. Lefebvre, "Reactive path deformation for nonholonomic mobile robots," *IEEE Trans. Robot. Autom.* **20**(6), 967–977 (2004).
15. D. Fox, W. Burgard and S. Thrun, "The dynamic window approach to collision avoidance," *IEEE Robot. Autom. Mag.* **4**, 22–23 (1997).
16. P. Ögren and N. E. Leonard, "A convergent dynamic window approach to obstacle avoidance," *IEEE Trans. Robot. Autom.* **21**(2), 188–195 (2005).
17. J. Huang *et al.*, "A model-based sound localization system and its application to robot navigation," *Robot. Auton. Syst.* **27**, 199–209 (1999).
18. E. Bicho, P. Mallet and G. Schöner, "Target representation on an autonomous vehicle with low-level sensors," *Int. J. Robot. Res.* **19**(5), 424–447 (2000).
19. S. B. Andersson, A. A. Handzel, V. Shah and P. Krishnaprasad, "Robot phonoaxis with dynamic sound-source localization," *IEEE International Conference on Robotics and Automation*, (2004) pp. 4833–4838.
20. K. Ohnihi, M. Shibata and T. Murakami, "Motion control for advanced mechtronics," *IEEE/ASME Trans. Mechatronics* **1**(1), 56–67 (1996).

https://doi.org/10.1017/S0263574709990919 Published online by Cambridge University Press